PHYSICAL REVIEW B **80**, 140506(R) (2009)

Stationary phase-kink states and dynamical phase transitions controlled by surface impedance in terahertz wave emission from intrinsic Josephson junctions

Yoshihiko Nonomura*

Computational Materials Science Center, National Institute for Materials Science, Tsukuba, Ibaraki 305-0047, Japan

(Received 30 June 2009; revised manuscript received 3 September 2009; published 9 October 2009)

As possible states to characterize THz wave emission from intrinsic Josephson junctions without external fields, the McCumber-like state and π-phase-kink state have been proposed. In the present Rapid Communication it is numerically shown that both states are stationary according to the bias current J and surface impedance Z. The McCumber-like state is stable for low J and small Z. For higher J, the π-phase-kink state accompanied with symmetry breaking along the c axis is stable even for $Z=1$, though strong emission in the vicinity of cavity resonance points only takes place for larger Z. Different emission behaviors for $Z=1$ and 10 are precisely compared. The dynamical phase diagram for $1 \leq Z \leq 10$ and the optimal value of Z for the strongest emission are also evaluated.

DOI: 10.1103/PhysRevB.80.140506 PACS number(s): 74.50.+r, 74.25.Nf, 85.25.Cp

I. INTRODUCTION

Emission from intrinsic Josephson junctions (IJJs) such as $Bi_2Sr_2CaCu_2O_8$ (BSCCO) has been intensively studied as a candidate of stable source of continuous terahertz electromagnetic wave. Although emission controlled by flow of Josephson vortices[1] had been investigated numerically,[2–4] experimental realization of such emission[5] had been quite difficult. Recently more evident emission from IJJs without external fields was reported experimentally,[6] and two types of states were proposed theoretically in order to explain the emission. One is the McCumber-like state (Ohmic and translational invariant along the c axis),[7] and another is the π-phase-kink state (non-Ohmic with nontrivial symmetry breaking along the c axis).[8] These proposals share the basic framework,[1,9] and difference in results is due to choice of the boundary condition. In the present Rapid Communication we start from a simplified version[4] of the dynamical boundary condition[10] used in Ref. 7, and gradually introduce effect of the surface impedance.[8]

II. MODEL AND FORMULATION

Differently from emission in external fields, dimensional reduction along the field cannot be justified anymore in zero-field emission. Actually, the above two research groups have already generalized their results to three dimensions.[11,12] Nevertheless, such generalization did not resolve the discrepancy between them. Then, in order to clarify the origin of this discrepancy, we concentrate on the two-dimensional modeling assuming uniform solutions along the y axis.[7,8] That is, we solve the following differential equations:[3]

$$\partial_{x'}^2 \psi_{l+1,l} = (1 - \zeta\Delta^{(2)})(\partial_{t'} E'_{l+1,l} + \beta E'_{l+1,l} + \sin \psi_{l+1,l} - J'), \tag{1}$$

$$\partial_{t'} \psi_{l+1,l} = (1 - \alpha\Delta^{(2)}) E'_{l+1,l}, \tag{2}$$

where the subscript "$l+1,l$" denotes quantities in the insulating layer between the l-th and $(l+1)$th superconducting layers, and the operator $\Delta^{(2)}$ is defined in $\Delta^{(2)} X_{l+1,l} \equiv X_{l+2,l+1} - 2X_{l+1,l} + X_{l,l-1}$. The electric field and gauge-invariant phase difference controlled by the dc bias current J are basic quantities, and the magnetic field is obtained from $\partial_{x'} \psi_{l+1,l} = (1 - \zeta\Delta^{(2)}) B'_{l+1,l}$. In these formulas the following scaled quantities are used:

$$x' = \frac{x}{\lambda_c}, \quad t' = \omega_p t, \quad J' = \frac{J}{J_c}, \tag{3}$$

$$E'_{l+1,l} = \frac{\sigma_c}{\beta J_c} E^z_{l+1,l}, \quad B' = \frac{2\pi\lambda_c d}{\phi_0} B, \tag{4}$$

$$\zeta = \frac{\lambda_{ab}^2}{sd}, \quad \alpha = \frac{\epsilon'_c \mu^2}{sd}, \quad \beta = \frac{\sqrt{\epsilon'_c}\sigma_c \lambda_c}{\epsilon_c c}, \tag{5}$$

$$\omega_p = \frac{c}{\sqrt{\epsilon'_c}\lambda_c}, \quad J_c = \frac{\phi_0}{2\pi\mu_0 \lambda_c^2 d}, \tag{6}$$

with the penetration depths $\lambda_{ab}=0.4$ μm and $\lambda_c=200$ μm, thickness of superconducting and insulating layers $s=3$ Å and $d=12$ Å, respectively, Debye length $\mu=0.6$ Å, dielectric constant of the junction $\epsilon'_c=\epsilon_c/\epsilon_0=10$ with permittivity of the junction ϵ_c, plasma frequency ω_p, conductivity σ_c, flux quantum ϕ_0, and critical current J_c, following the material parameters of BSCCO in Ref. 3. They give $\alpha=0.1$ and $\beta=0.02$ is taken here.

Width of the junction $L_x=86$ μm is comparable to those of samples used in experiments.[6] Since direct simulation of several hundreds of layers is difficult, the periodic boundary condition along the c axis corresponding to effectively infinite layers is introduced instead. In addition to calculations for the number of layers $N=4$, some systems with $N=8$ or 12 are analyzed to confirm numerical consistency. In place of considering outside of IJJs, the dynamical boundary condition on edges[10] is introduced. For infinite and uniform layers, this boundary condition is simplified[4] as the relation between the dynamical part of scaled boundary fields $\tilde{B}'_{l+1,l}$ and $\tilde{E}'_{l+1,l}$,

$$\partial_{x'} \psi_{l+1,l} = B'_{\mathrm{ext}} + \tilde{B}'_{l+1,l}, \tag{7}$$

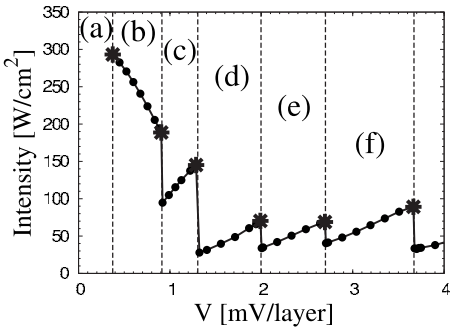

FIG. 1. Voltage dependence of emission intensity for $Z=1$. Regions (a)–(f) are divided by jumps of intensity (dashed lines), and the data points with star symbols correspond to the voltages at which Figs. 2 and 3 are drawn.

$$\partial_{t'}\psi_{l+1,l} = \langle E'_{l+1,l}\rangle + \tilde{E}'_{l+1,l}, \tag{8}$$

$$\tilde{E}'_{l+1,l} = \mp Z\tilde{B}'_{l+1,l}, \quad Z = z\sqrt{\epsilon'_c/\epsilon'_d}, \tag{9}$$

with the dielectric constant of dielectrics ϵ'_d. The factor $z(\geq 1)$ is considered[13] to appear when the wavelength λ of emitted electromagnetic wave is much longer than the thickness of junctions L_z, which usually holds in experiments, as $z \approx \lambda / L_z$. Effect of impedance mismatch on the edges is also included in Z. When surface fields are not uniform along the c axis, Z depends on wave number and frequency in the exact expression.[10,13,14] Width of the sample L_x is divided into 80 numerical grids.

In numerical evaluation of stationary states, procedure for parameter sweep is essential. One possible approach is to start from a zero-current state and gradually vary currents[8] similarly to experiments. However, it may not be suitable for study on stationary states. Simulated time scale is much shorter than that in experiments, and accidental trap by metastable condition may be held during gradual change of current. Then, we start from random configurations for each current and check the consistency of results. Continuous data obtained from independent initial conditions strongly suggest that the results are stationary ones. Since each data point is independent, convergence of calculations can be easily checked by additional simulations. In order to obtain convergent results from random initial configurations precise algorithm with automatically optimized time steps is essential, and the RADAU5 ODE solver[15] is utilized for this purpose.

Even if this precise algorithm is used, self-consistent evaluation of $\langle E'_{l+1,l}\rangle$ is still difficult. We first fix the static value of the surface electric field in order to obtain a stationary state under this constraint, and then determine $\langle E'_{l+1,l}\rangle$ self-consistently from this stationary state. When the determined average value and amplitude of the surface electric field are denoted as E_{av} and ΔE, respectively, strong emission state can be obtained from an initial static value E_{ini} satisfying $E_{ini} < E_{av} - \Delta E$. This condition looks consistent with the fact that strong emission state can only be observed in current-increasing process during gradual variance of current.[8]

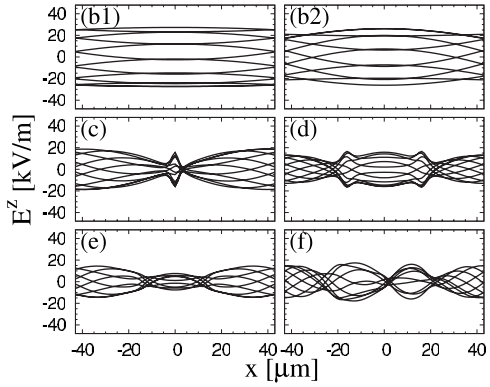

FIG. 2. A series of snapshots of the dynamical part of electric fields in a layer of IJJ for some typical values of voltages (per layer) for $Z=1$: (b1) 0.37, (b2) 0.90, (c) 1.29, (d) 1.99, (e) 2.70, and (f) 3.66 mV.

III. NUMERICAL RESULTS FOR $Z=1$

This condition is typically realized for $z=1$ and $\epsilon'_c = \epsilon'_d$, namely no impedance mismatch in an infinite system. Voltage dependence of intensity, namely the strength of Poynting vector, is shown in Fig. 1. Intensity takes maximum at the onset of emission, and there exist several abrupt jumps which correspond to change of modes of electromagnetic waves in IJJs. The range of voltage shown in Fig. 1 is divided into six regions, (a)–(f), and snapshots of electric field in each region are displayed in Figs. 2(b)1–2(f), respectively.

Retrapping region (a) is characterized by vanishing voltage for finite bias current. In region (b), spatial dependence of electric fields is small and in-phase motion occurs in all layers, which resembles the McCumber state.[16] This McCumber-like state was automatically chosen when translational invariance along the c axis is assumed.[7] A series of snapshots of electric fields for the lowest and highest voltages in this region are shown in Figs. 2(b)1 and 2(b)2, respectively. They show that spatial dependence of electric fields increases as the voltage increases. In the region (c), the state with a π-phase kink is favored. This state accompanies symmetry breaking of phases along the c axis [see Fig. 3(c)].

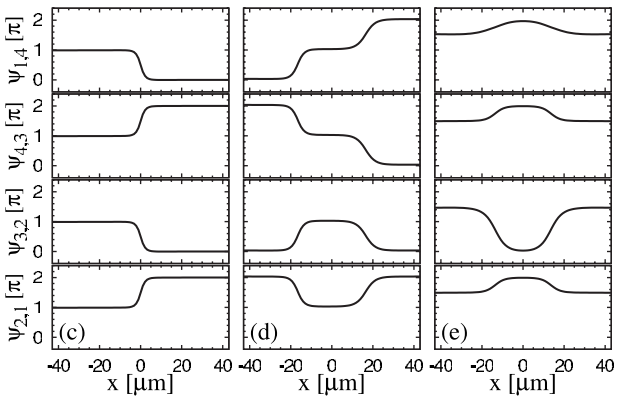

FIG. 3. Gauge-invariant phase differences in all insurating layers corresponding to the voltages for Figs. 2(c)–2(e). $\pi/2$- and $3\pi/2$-phase kinks are stabilized in Fig. 3(e).

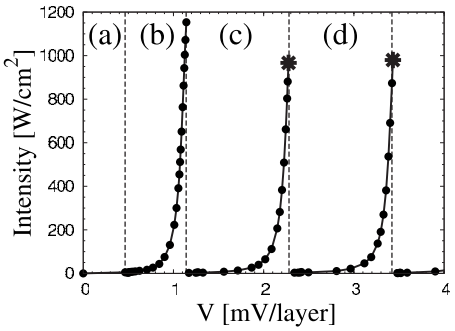

FIG. 4. Voltage dependence of emission intensity for $Z=10$. Intensity is diverging toward the cavity resonance points $V=1.14n$ [mV/layer] (dashed lines) with the integer n to specify cavity modes. Other than the retrapping region (a) are divided by these voltages, and the data points with star symbols correspond to the voltages at which Fig. 5 is drawn.

Such a state was observed for a large and complex value of Z (Ref. 8) or for spatially inhomogeneous J_c (Ref. 17) previously. In regions (d) and (f), similar symmetry-breaking states with increasing number of π-phase kinks are stable [see Fig. 3(d): the two-kink case with period 4]. Region (e) is rather special, where two non-π-phase kinks are stabilized. For $N=4$, three layers have $+\pi/2$- and $-\pi/2$-phase kinks and one layer has $+3\pi/2$- and $-3\pi/2$-ones [see Fig. 3(e)]. Structure of non-π-phase kinks depends on N. For example, for $N=6$ four layers with $\pm 2\pi/3$-phase kinks and two layers with $\mp 4\pi/3$ ones. Note that it is not the purpose of the present study to check N-dependence of emission states in this region in detail.

IV. NUMERICAL RESULTS FOR $Z=10$

Voltage dependence of intensity shown in Fig. 4 is diverging in the vicinity of the cavity resonance points (dashed lines), which is quite different from the behavior for $Z=1$ (see Fig. 1). The McCumber-like state never appears, and standing-wave-like behavior (see Fig. 5) occurs near the cavity resonance points. Origin of such behavior can be understood from the J-V curve shown in Fig. 6. For $Z=1$ (shown in the inset), the J-V curve (solid line) almost coincides with the Ohm's law (dashed line), which means that most of input current changes to Joule heat. While for $Z=10$, this curve apparently goes away from the Ohm's law in the vicinity of the cavity resonance points, where the voltage almost saturates when the current increases and the excess energy is emitted as electromagnetic waves.

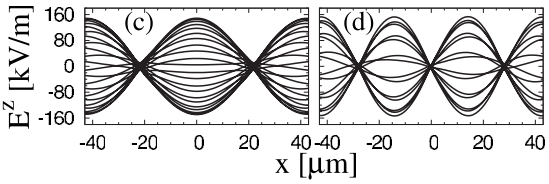

FIG. 5. A series of snapshots of the dynamical part of electric fields in a layer of IJJ at intensity peaks for $Z=10$: (b) 2.28 ($n=2$) and (c) 3.43 mV ($n=3$) with the integer n to specify cavity modes.

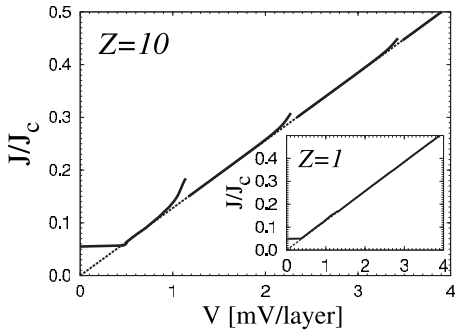

FIG. 6. J-V curve for $Z=1$ (inset) and $Z=10$. Dashed lines represent the Ohm's law for the normal current.

V. NUMERICAL RESULTS FOR OTHER Z

Emission behaviors for $Z=1$ and 10 are quite different, and it is interesting what happens for intermediate values of Z. Then, the dynamical phase diagram in the Z-J plane is given in Fig. 7. Apparently, the McCumber-like state (denoted by M) is stable only for a limited parameter region: $Z<5$ and $0.05<J/J_c<0.12$. Boundary of the two-incommensurate-phase-kink state (denoted by I_2) is evaluated for $N=4$, and quantitative change may occur for larger N. Important thing is that this phase is stable only for $Z<2$, and that most regions of the dynamical phase diagram are covered by the π-phase-kink states (denoted by K_n, n: number of kinks). Intensity of emission at the K_1-K_2 boundary becomes comparable to that at the R-M boundary (R: retrapping) for $Z\approx 3$, and boundaries between different π-phase-kink states become almost independent of Z for $Z\geq 3$, where strong emission governed by the ac Josephson relation is observed.

Finally, surface-impedance dependence of emission intensity for larger Z is investigated. That is, stationary emission is optimized for various values of Z, which are varied from 3 to 10 000. Maximum intensity in each cavity mode is observed, and all the maximum values are plotted versus Z in Fig. 8. The strongest emission is observed at $Z\approx 50$ for $n=1$, $Z\approx 80$ for $n=2$, and $Z\approx 100$ for $n=3$, respectively.

VI. DISCUSSIONS

In Ref. 8, large surface impedance $|Z|=1000$ was introduced as a consequence of large z due to small thickness of

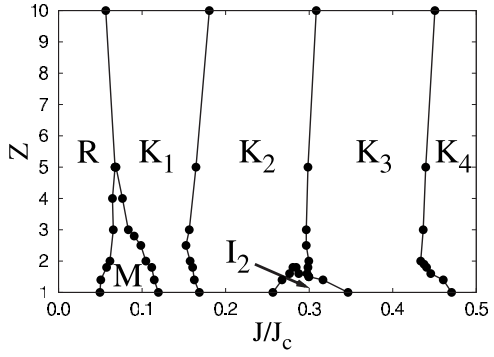

FIG. 7. Dynamical phase diagram in the Z-J plane. R, M, K_n, and I_m denote the retrapping, McCumber-like, $n-\pi$-phase kink, and m-incommensurate-phase-kink states, respectively.

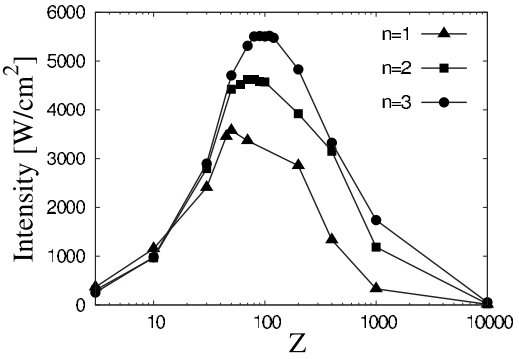

FIG. 8. Surface-impedance dependence of maximum intensity in a semilog scale for first three cavity modes: $n=1$ (triangles), 2 (squares), and 3 (circles).

the IJJ,[13] though this surface effect may be cancelled[18] by penetration of magnetic fields from transverse directions, which is neglected in two-dimensional modeling. Then, stability of standing-wave-like behavior for $Z \geq 3$ is important, because emission from an infinite IJJ to vacuum ($\epsilon_c'=10, \epsilon_d'=1$ and $z=1$) results in $Z=\sqrt{10}$ and satisfies $Z>3$.

Z and n dependence of emission intensity can be explained as follows: Electromagnetic wave in IJJs becomes closer to standing wave for larger Z, and amplitude of the electric field increases. On the other hand, the amplitude cannot exceed its static value and saturates as Z further increases, and intensity decreases because the magnetic field is inversely proportional to Z. As larger value of n is taken, static value of the electric field increases and the optimal point of emission shifts toward larger Z.

Although phase difference radically varies from layer to layer in the phase-kink states as shown in Fig. 3, surface fields are almost uniform for any values of Z. This fact shows that the assumption with constant Z in Eq. (9) is a good approximation within the present framework.

VII. SUMMARY

In the present Rapid Communication terahertz wave emission from intrinsic Josephson junctions without external fields is investigated numerically, and discrepancy between two previous studies based on the two-dimensional modeling[7,8] is resolved. The surface impedance Z is found out to be essential for characterization of emission behavior. For $Z=1$, the McCumber-like state is stable for low dc bias currents as reported in Ref. 7, and this emission state is specific to small Z. Even for $Z=1$, π-phase-kink states become stationary for higher currents. Since the π-phase-kink states require symmetry breaking of phases between insulating layers, it was not observed in Ref. 7, where in-phase motion was assumed *a prior*. Although large Z is not necessary for stable π-phase-kink states, strong emission from standing-wave-like states does not occur for $Z=1$, and such emission is observed at least for $Z \geq 3$. This condition can be satisfied only by the impedance mismatch between IJJs and electrodes, namely the emission from an infinite IJJ to vacuum gives $Z=\sqrt{10}$. Emission behaviors for $Z=10$ are qualitatively similar to those in Ref. 8 characterized by sharp intensity peaks at the cavity resonance points. The strongest emission is observed for $Z \approx 50 \sim 100$ slightly depending on the cavity mode n, and such behavior can be explained by saturation of the electric field.

ACKNOWLEDGMENTS

The present author would like to thank M. Tachiki, T. Koyama, X. Hu, and S. Lin for helpful comments. This work was partially supported by Grant-in-Aids for Scientific Research (C) No. 20510121 from JSPS and by the CTC program under JSPS.

*nonomura.yoshihiko@nims.go.jp

[1] T. Koyama and M. Tachiki, Solid State Commun. **96**, 367 (1995).
[2] M. Machida, T. Koyama, A. Tanaka, and M. Tachiki, Physica C **330**, 85 (2000); M. Machida, T. Koyama, and M. Tachiki, *ibid.* **362**, 16 (2001).
[3] M. Tachiki, M. Iizuka, K. Minami, S. Tejima, and H. Nakamura, Phys. Rev. B **71**, 134515 (2005).
[4] S. Lin, X. Hu, and M. Tachiki, Phys. Rev. B **77**, 014507 (2008).
[5] K. Kadowaki, I. Kakeya, T. Yamamoto, T. Yamazaki, M. Kohri, and Y. Kubo, Physica C **437-438**, 111 (2006); M.-H. Bae, H.-J. Lee, and J.-H. Choi, Phys. Rev. Lett. **98**, 027002 (2007).
[6] L. Ozyuzer, A. E. Koshelev, C. Kurter, N. Gopalsami, Q. Li, M. Tachiki, K. Kadowaki, T. Yamamoto, H. Minami, H. Yamaguchi, T. Tachiki, K. E. Gray, W.-K. Kwok, and U. Welp, Science **318**, 1291 (2007); K. Kadowaki, H. Yamaguchi, K. Kawamata, T. Yamamoto, H. Minami, I. Kakeya, U. Welp, L. Ozyuzer, A. Koshelev, C. Kurter, K. E. Gray, W.-K. Kwok, Physica C **468**, 634 (2008); see also K. Lee, W. Wang, I. Iguchi, M. Tachiki, K. Hirata, and T. Mochiku, Phys. Rev. B **61**, 3616 (2000).
[7] H. Matsumoto, T. Koyama, and M. Machida, Physica C **468**, 654 (2008); H. Matsumoto, T. Koyama, M. Machida, and M. Tachiki, *ibid.* **468**, 1899 (2008).
[8] S. Lin and X. Hu, Phys. Rev. Lett. **100**, 247006 (2008).
[9] S. Sakai, P. Bodin, and N. F. Pedersen, J. Appl. Phys. **73**, 2411 (1993); S. Sakai, A. V. Ustinov, H. Kohlstedt, A. Petraglia, and N. F. Pedersen, Phys. Rev. B **50**, 12905 (1994).
[10] L. N. Bulaevskii and A. E. Koshelev, Phys. Rev. Lett. **97**, 267001 (2006); J. Supercond. Novel Magn. **19**, 349 (2006).
[11] T. Koyama, H. Matsumoto, and M. Machida, J. Phys.: Conf. Ser. **129**, 012026 (2008); H. Matsumoto, T. Koyama, and M. Machida, *ibid.* **129**, 012028 (2008).
[12] X. Hu and S. Lin, Phys. Rev. B **78**, 134510 (2008); S. Lin and X. Hu, *ibid.* **79**, 104507 (2009).
[13] A. E. Koshelev and L. N. Bulaevskii, Phys. Rev. B **77**, 014530 (2008).
[14] L. N. Bulaevskii and A. E. Koshelev, Phys. Rev. Lett. **99**, 057002 (2007).
[15] http://www.unige.ch/~hairer/software.html
[16] R. Kleiner, T. Gaber, and G. Hechtfischer, Phys. Rev. B **62**, 4086 (2000).
[17] A. E. Koshelev, Phys. Rev. B **78**, 174509 (2008).
[18] M. Tachiki, S. Fukuya, and T. Koyama, Phys. Rev. Lett. **102**, 127002 (2009).